Colloid and Polymer Science
https://doi.org/10.1007/s00396-020-04782-6

ORIGINAL CONTRIBUTION

Organoclay/conjugated polymer nanocomposites: structural, thermal, and electrical properties

Leila Mouacher[1] · Ahmed Yahiaoui[1] · Aicha Hachemaoui[1] · Abdelkader Dehbi[2] · Ali Mustapha Benkouider[1]

Received: 4 May 2020 / Revised: 30 October 2020 / Accepted: 5 November 2020

Abstract

A detailed study about the chemical oxidative polymerization of aniline with/or 2-aminothiazole in the presence of an organoclay has been reported. The first step achieved was the organophilization of the clay by using cetrimonium bromide (CTAB) surfactant; then, the nanocomposites were synthesized with the addition of a stoichiometric amount of ammonium persulfate (APS) in aqueous solution. The effect of varying the reaction time and oxidant/monomer and co-monomer molar ratio on the polymer yield was investigated. The resulting nanocomposites were fully characterized using FTIR and UV-Vis measurements which have shown that polymerizations have been carried out. XPS has certified that the clay has undergone a cationic exchange of sodium by the cationic surfactant. X-ray diffraction confirmed that polymers/copolymers were largely incorporated into the clay. Good electrical response and improved thermal stability for the synthesized nanocomposites have been observed.

Keywords Nanocomposite · Clay · Copolymers · Conducting polymers · Surfactants

Introduction

The absorption of different types of macromolecules onto lattice layers clays permitting in situ polymerizations yielding clay/conjugated polymer nanocomposites have garnered an increasing interest in the scientific community, These organic/inorganic hybrid materials with improved mechanical, thermal, and gas barrier properties [1, 2] have a wide field of application, including electronic, nanoelectronic, and biomedical devices [3, 4]; moreover, they were found to be remarkable materials for antistatic coatings [5], anti-corrosion coatings [6], electrochromic devices [7], supercapacitors, and actuators [8, 9].

As clays are generally hydrophilic and naturally incompatible with organic materials, the preliminary step in our study consists of an alteration of the polarity of the Maghnite; an effective nontoxic and ecological Algerian montmorillonite, used as a catalyst in several works [10, 11], through cation exchange in the interlayer space: by inserting a sodium cation, the silicate layer thickness which is normally about 7 to 10 Å increases due to their structural nature, swelling, and cation exchange capacity CEC = 90 meq/g [12–14]; the organophobic nature of these inorganic-host-layered material makes the homogeneous mixture with the polymer matrix difficult or nearly impossible,; however, it can be done by the addition of compatibilizing agents such as alkylammonium ions to improve its compatibility with organic polymers [15], increasing its surface interlayer to 19.35 Å and allowing the dispersion of the organic phase [16]; there are generally three methods used for preparing a polymer/clay nanocomposite: intercalation of the polymer from a solution, intercalation of melt blending, and in situ polymerization [17]; it is the latter in which we are most interested in this study; it consists of mixing the clay with monomers before starting the polymerization permitting the growth of the polymer chain inside the silicate galleries.

2-Aminothiazole is a five-membered heterocyclic monomer, combining the characteristics of pyrrole, thiophene, and aniline, Sayyah et al. [18, 19] investigated kinetic study of chemical and electrochemical polymerization of thiazoles and aniline derivatives substituted in the meta and ortho position in acidic medium; they confirmed that the polymer chain of PAT and its derivatives progressed via the oxidation of the

✉ Abdelkader Dehbi
abdelkader.dehbi@univ-tiaret.dz

[1] Laboratory of Organic Chemistry Macromolecular and Materials, Faculty of Exact Sciences, University of Mascara, 29000 Mascara, Algeria

[2] Engineering Physics Laboratory, University of Tiaret, 14000 Tiaret, Algeria

group amine -NH_2; on the other hand, Ciftci et al. [20] suggested a ring opening polymerization using $FeCl_3$ $6H_2O$ in 1,4-dioxane. The advantage of polythiazoles compared to other polyheterocycles lies in their temperature resistance, rapid (electro)reduction, their large choice of reactive functional groups, and their semi-conducting properties [21, 22] that range between 10^{-4} and 10^{-8} S/cm [18, 22]; there is only few published works on PAT nanocomposites; in the presence of silica nanoparticles, the poly(2-aminothiazole)–silica nanocomposite was prepared by chemical oxidative polymerization [23]; furthermore, PAT graphene oxide composite is an efficient nanoadsorbent for extraction of toxic Cr(VI) ions and Hg(II) in aqueous solutions [24].

In our study, a copolymerization between 2-aminothiazole and aniline was investigated; as we know, polyaniline is one of the most used conductive polymer with a broad range of applications, in various hi-tech aspects, especially for electrical and electronic industrial applications; nevertheless, this polymer with outstanding properties, high electrical conductivity, near to that to the metal, mechanical stability, and strong thermal resistance [25], has low or almost nonexistent solubility in common solvents, affecting thus its process ability and restricted its applications, which is the biggest drawback of this polymer; it may be synthesized through different synthetic routes, electrochemical and chemical polymerizations [26]; the chemical oxidative polymerizations of aniline have been reported using various oxidant/solvent systems [27]; in our case, the nanocomposite was prepared by in situ polymerization of 2-aminothiazole and/or aniline; the monomers was first mixed to the organoclay, modified with cationic surfactant, cetyltrimethylammonium (CTAB) in aqueous solution, followed by a chemical oxidative polymerization with the addition of ammonium persulfate (APS) oxidant (Fig. 1); thus, the first objective of our work was to synthesize a new microstructured conductive/nanocomposite with high conversion; then, a kinetic study was investigated; the effects of initiator concentration and polymerization time on the polymer yield were studied. The polymer/organoclay nanocomposites and reference materials were confirmed with series of characterizations such as Fourier transform infrared spectroscopy (FTIR), UV-Vis, X-ray diffraction, and XPS. The solubility of our products was tested in common organic solvents as well as in acidic and basic solutions. Moreover, the electrical behavior and the thermal stability of the nanocomposites were also reported.

Experimental

Characterization

FTIR spectra were recorded using a Bruker Alpha spectrophotometer; the FTIR spectrum ranged from 4000 to 450 cm^{-1} at a resolution of 4 cm^{-1}.

UV-visible measurements were recorded using a Hitachi U-3000 spectrophotometer; a solution of N,N-diméthylformamide (DMF) was used for recording the spectrum.

XRD analysis of the powder nanocomposites was carried out at room temperature on an X'pert Pro diffractometer (Panalytical Company) operating at 40 kV, 40 mA using Co Kα radiation source (λ = 1.7902 Å) at the rate of 2° min"1 in the 2 tetha (2θ) range of 2.0–80°.

XPS were recorded with a Thermo VG Scientific ESCALAB 250 spectrometer (East Grinstead, U.K.) equipped with a monochromatic Al Kα X-ray source (1486.6 eV and 650 μm spot size). The specimens were pressed against insulating double-sided adhesive tape on sample holders and pumped overnight in the fast entry lock at ~5 × 10–8 mbar. The pass energy was set at 150 and 40 eV for the survey and the narrow scans, respectively. Charge compensation was achieved with an electron flood gun operated in the presence of argon at a partial pressure of 2 × 10–8 mbar in the analysis chamber. The spectra were calibrated against the C–C/C–H C 1s component set at 285 eV.

Transmission electron microscopy (TEM) analyses were carried out using a JEOL microscope, model (JEM-2010) 200 kV.

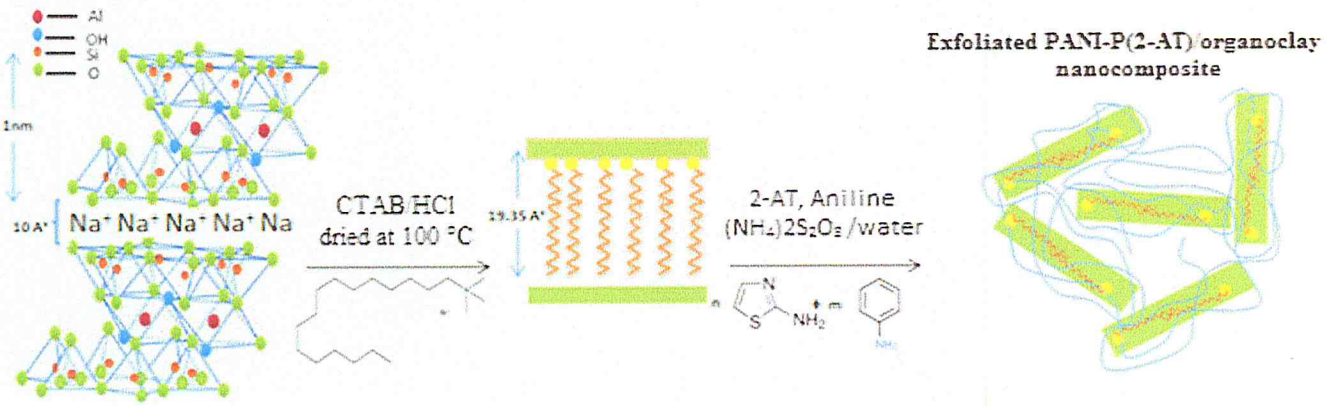

Fig. 1 In situ polymerization of aniline and 2-aminothiazole catalyzed by ammonium persulfate

Thermogravimetric analyses are made using TGA 4000 Peking Elmer; it is necessary just before the polymer powder is dried, to raise the temperature with a step of 10 °C until the temperature 850 °C is reached.

Electrical conductivity of solutions of the prepared compounds in DMF was measured at room temperature, by using Hall effect measurement.

Materials and methods

Raw-Maghnite clay deposits of Maghnia is supplied by a local company (ENOF Maghnia in Western of Algeria) and purified with distilled water (Clay ion-exchange capacity = 92 mequiv/100 g). 2-Aminothiazole (2-AT) 97%, aniline (AN) 99.5%, cetrimonium bromide (CTAB) 99%, sodium chloride powder (NaCl) 97%, hydrochloric acid (HCl) 37%, ethanol 99%, dimethylformamide (DMF) 97.5%, and ammonium persulfate (APS) 98% were all used as purchased from Aldrich Chemical St. Louis, MO, USA without any further purification unless specified.

Preparation of the Maghnite-Na^+ (M-Na^+)

M-Na^+ was prepared as follows: 20 g of purified Maghnite are immersed in an Erlenmeyer flask together with 500 ml of 1 M NaCl; the mixture was kept under magnetic stirring at 250 rpm, at room temperature for 24 h, after decantation of the suspension; the supernatant is washed several times with distilled water to remove excess salt, until the disappearance of the chlorides Cl^- ions tested by silver nitrate $AgNO_3$, Mag-Na^+ is then filtered, dried and ground with a mortar until obtaining a fine powder and then dried at 105 °C overnight before the day of the experiment.

Preparation of the organo-modified clay (OM)

OM was prepared according to several protocols, in acidic and aqueous solutions [28]. In a 500 ml graduated flask, 5 ml of hydrochloric acid HCl 1 N is introduced; the remaining volume is filled up with distilled water, 10 mmol of CTAB is added to the acidic solution which is poured into an Erlenmeyer flask containing a magnetic stirrer bar, after 2 h of stirring; 10 g of M-Na^+ prepared previously is added to the mixture. The solution is stirred at room temperature for 24 h to promote cation exchange; at the beginning of the reaction, we notice the swelling of the clay. After having filtered the OM and washed several times with a mixture of water/ethanol 50/50 heated to 60 °C, the organoclay is dried at 100 °C, ground with a mortar, and kept shielded from the air.

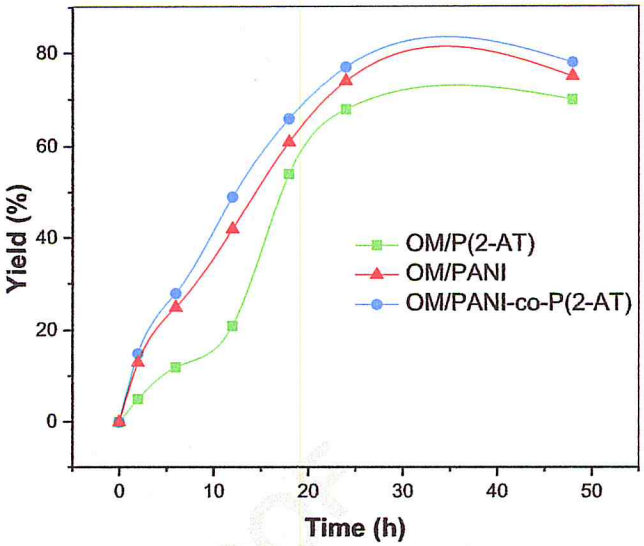

Fig. 2 Effect of the reaction time on the yield of nanocomposites. At 50 °C, 2-AT_0 = An_0 = 15 mmol, APS_0 = 10 mmol

Synthesis of OM/PANI, OM/P(2-AT), and OM/PANI-co-P(2-AT) nanocomposites

To obtain the nanocomposites, 0.25 g of OM was added to a vigorously stirred solution of 15 mmol of 2-aminothiazole and/or aniline monomer with equivalent molar ratio (50/50); it was stirred for 30 min, and the chemical polymerization began by the dropwise addition of 10 ml of ammonium persulfate $(NH_4)2S_2O_8$ solution (10 mmol); the system was kept at 5 °C for two hours; then, the reaction was left at 50 °C for 24 h to achieve high molecular weight polymers and copolymers species; it is noted that the color of the solution changed from orange to dark brown; the precipitates obtained are filtered and rinsed with dionised water in order to remove traces of unreactive monomers and oxidant and then dried under vacuum at 50 °C for 1 day. The solubility of OM/PANI,

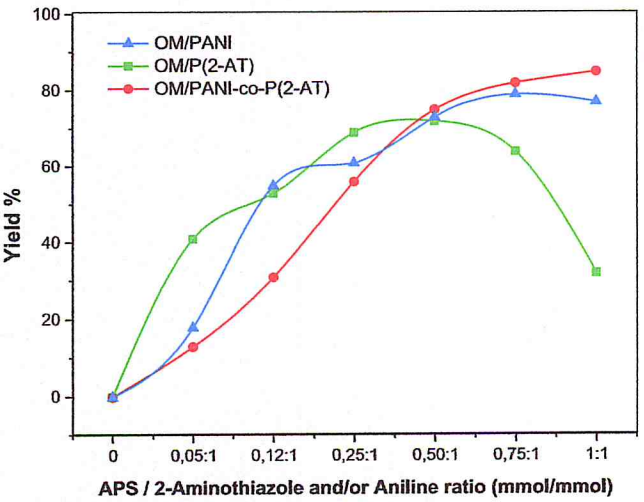

Fig. 3 Effect of initiator on polymers yields. At 50 °C, 2-AT_0 = An_0 = 15 mmol for 24 h

OM/P(2-AT), and OM/PANI-co-P(2-AT) was checked, in many solvents such as Éthylène glycol, NMP, DMSO, and DMF and it was found to be soluble.

The investigation of synthesis conditions of the synthesized nanocomposites

To optimize the different parameters of the polymerization process leading to improved properties, several reaction conditions were tried in order at 50 °C in aqueous solution; the yield of the oxidative polymerization products depending on the effects of various parameters, such as the reaction time and the initial concentrations of oxidant (APS), is given in Figs. 2 and 3.

Effect of polymerization time on the polymer yield

The effect of reaction time on the rate of oxidative synthesis of nanocomposites was studied under the optimum reaction conditions: $AN_0 = 2\text{-}AT_0 = 15$ mmol, $APS_0 = 10$ mmol at fixed temperature 50 °C; the reaction time for the polymerization of nanocomposites was varied from 2 to 48 h. In all the cases, plots of % yield versus polymerization time indicated that an increase in reaction time resulted in an increase in the polymer yield as shown in Fig. 2. The total conversions (71, 69, and 74%) of PANI, P(2-AT), and PANI-co-P(2-AT), respectively, was achieved after 24 h; below this duration, the polymer conversion is incomplete, and beyond it, polymers yields reached stationary phases and remain constant; consequently, optimum polymerization time was selected as 24 h, which is evidently caused by an increase in the medium viscosity through the formation of extended polymer chains.

Effect of APS concentration on the polymer yield

Figure 3 shows the effect of APS/2-aminothiazole and/or aniline molar ratio on the yield of the polymerizations; the effect of APS concentration was studied at fixed monomers amount (15 mmol), and a fixed temperature 50 °C for 24 h. Wide molar range of APS has been tested; in the case of PANI and PANI-co-P(2-AT), polymer yields increased with the increase of APS amount; the conversion reached nearly 80% after 24 h and leveled off at 1 : 1 M ration (APS = 15 mmol), whereas significant reduction of the polymer conversion was recorded about 50% for P(2-AT) as shown in Fig. 3; this result may be explained owing to the formation of low molecular weight oligomers; indeed, the presence of excess oxidant is not favored to be used and will cause over-oxidation by initiating a higher number of active centers species, decreasing thus the polymer chain growth which split into smaller molecular chains which dissolves in the solvent and lost during filtration.

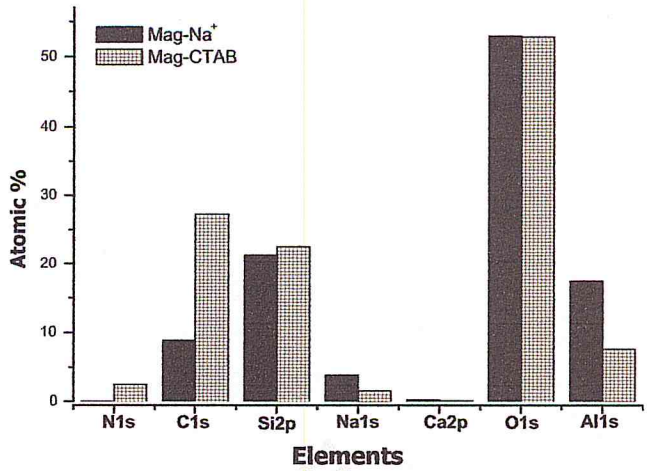

Fig. 4 Surface element atomic percentage of M-Na^+ and OM determined by XPS

Results and discussion

Characterization of the organoclay OM

To demonstrate the intercalation of the cationic surfactant between clay sheets, the modified clay was investigated by XPS, FTIR, and DRX. The atomic composition for the sodium clay (M-Na^+) before and after CTAB cation exchange is exhibited in Fig. 4. The major components of the atomic surface are Al 2p, Si 2p, C 1s, N 1s, O 1s, and Na 1s. The bar graph presents three significant changes between the two modified clays: (a) a huge increase of the carbon content arising from the CTAB incorporation into the clay galleries, (b) a large amount of sodium cation almost disappears from the organoclay confirming the cation exchange phenomenon of the sodium by the ammonium salt [29], and (c) nitrogen is the only marker

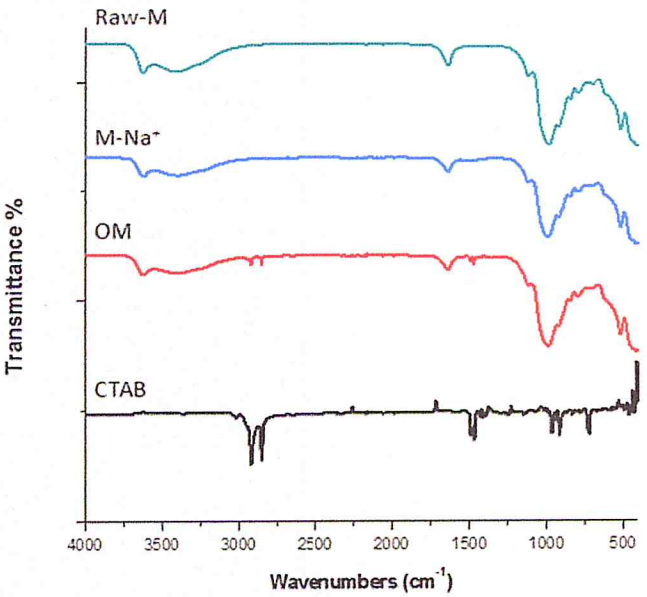

Fig. 5 FTIR adsorption spectra of raw Maghnite and its modified counterparts

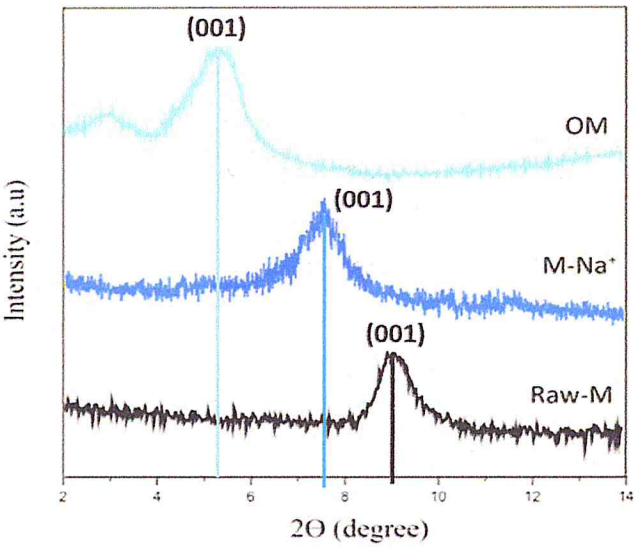

Fig. 6 X-ray diffraction patterns of raw Maghnite and its modified counterparts

element for the CTAB and is definitely nonexistent in the M-Na^+ composition, a significant increase is noticed from nil to a certain amount.

FTIR spectra of the raw-M, M-Na^+, CTAB, and OM are shown in Fig. 5; the absorption bands located at 3625 cm^{-1} and 1630 cm^{-1} are related to the stretching vibration of OH molecules of the octahedral layer and deformation bands of H–O–H bending of the physisorbed water, respectively; between 3405 and 3500 cm^{-1}, a broad band attributed to the Mg-O molecules of adsorbed water molecules in the Maghnite galleries, an intense band located in the 790–1050 cm^{-1} region characterizes the stretching vibration of the Si-O of the tetrahedral layer and the band appearing at 787 cm^{-1} is attributed to the deformation vibrations of Al-OH bands followed by the deformation bands of (Si-O-Al) at 524 cm^{-1} [30]. The intense band at 459 cm-1 is assigned to the Si-O-Al and Si-O-Mg coupled to OH vibration or Si- O bending vibrations [31, 32]. The effects of the process of intercalation of CTAB between the clay sheets on the FTIR spectrum are summarized as follows: the appearance of narrow bands near 2847 cm^{-1} and 2919 cm^{-1} is less intense compared to the CTAB spectra, which correspond to the elongation vibrations of alkyl chains (-CH_2 and -CH_3); we also observed a same band as on the spectrum of CTAB at 1471 cm^{-1} which is assigned to the C-N stretching vibration of the quaternary ammonium bond appears shorter with the surfactant intercalation; indeed, the concentration of CTAB as well as the length of its alkyl chains affect the intensity of the bands [33–35].

X-ray diffraction was used to investigate the intercalation of CTAB surfactant inside an intermediate layer of Maghnite, as shown in Fig. 6. The *d*-spacing values *d* (001) were calculated from the peak position of the X-ray diagram using the Bragg equation $d = 2\pi/q$, where q is the amplitude of the diffusion vector defined by $q = (4\pi/\lambda)\sin(\theta)$, λ is the wavelength of X-rays, and 2θ is the scattering angle [36]. There is a clear shift in peak position after the Na^+ insertion which corresponds to $2\theta = 7.42°$, thus, a slight increase in the d001 distance between the reticular planes, which goes from 11.9 Å for pristine clay to 12.45 Å in the M-Na^+; this expansion of interlayer space is due to the ease of introduction of ions between clay sheets; OM shows a significant displacement of the diffraction peak to a smallest angle $2\theta = 5.45°$, therefore a basal spacing of 19.14 Å. Beyond this concentration, the *d*-spacing reached the maximum $2\theta = 32$ Å [37]; a bimodal profile of two values 19 Å and 33 Å are obtained; in the first type of insertion, the introduced CTAB has probably adopted a paraffin type within the interlayer space of Maghnite [38]. In the second one, the ammonium groups stay fixed to the silicate layer while the chains in all-trans conformation point away from the surface [36]. This increase in basal spacing and shifting of 2θ indicates that alkylammonium surfactant was successfully incorporated into the interlayer galleries of Maghnite with simple cationic exchange helped by van der Waals forces between hydrocarbon chains and electrostatic repulsion between the hydrophilic heads of the surfactant [39, 40], resulting in an organophilic Maghnite, where the hydrophobic behavior arise mainly from the connection points between inter-particle and interaggregate [41].

Characterization of the nanocomposites

Surface element composition

Table 1 reports the surface elemental compositions of the interchanged clay: OM, P(2-AT), OM/PANI, and OM/ P(2-AT)-co-PANI; we notice the emergence of two major

Table 1 Composition (wt%) of OM/P(2-AT), OM/PANI, and OM/ P(2-AT)-co-PANI samples determined by XPS

Materials	N 1 s	C 1 s	O 1 s	Si2p	Al2p	Na1s	F1s	B1s	Ca	S2p	Ag2p
OM	0.12	8.55	59.83	20.06	8.28	2.79	–	–	0.49	–	–
OM/PANI	7.33	39.24	52.89	21.26	7.62	0.50	0.43	0.53	0.42	1.31	0.02
OM/P(2-AT)	13.72	19.53	44.56	15.15	5.97	0.13	0.38	–	–	7.35	0.04
OM/ P(2-AT)-co-PANI	14.02	37.41	41.05	14.81	5.78	0.06	–	–	–	4.81	0.04

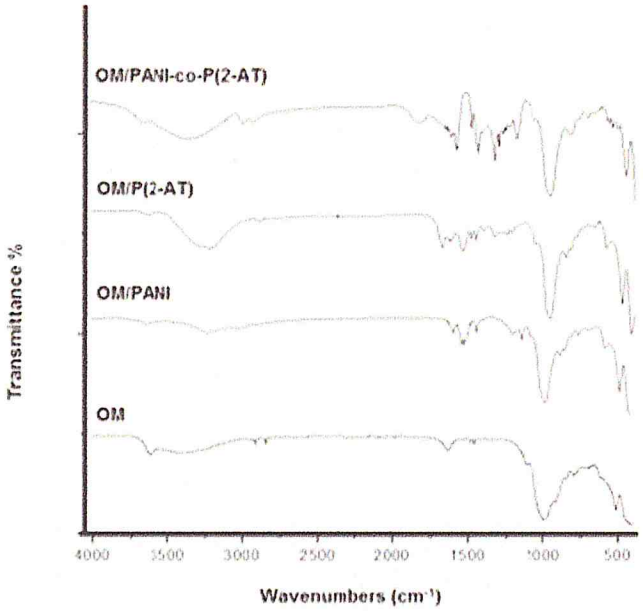

Fig. 7 FTIR spectra of OM, OM/PANI, OM/P(2-AT), and OM/PANI-co-P(2-AT) nanocomposites

elements almost inexistent in the organo-modified clay, the N1s and the S2p; moreover the relative intensity of the C1s increases with the carbon surface content; this clear change is due to the attachment of the polymer to the clay; the amount of the sodium decreases in the nanocomposites rigorously, by contrast to the Si/Al ratio which is almost constant.

FTIR spectra

Figure 7 exhibited the FTIR spectra of OM, OM/P(2-AT), OM/PANI, and OM/PANI-co-P(2-AT) nanocomposites. The characteristic infrared bands of OM and polymer/OM nanocomposites are listed in Table 2.

FTIR spectra of OM/Polymer nanocomposites present similar bands as those of the organo-modified Maghnite; the presence of kaolinite is justified by the planar stretching bands at 3625 cm^{-1} belonging to OH groups of the octahedral layer; we notice that the intensity of these peaks is not affected by the intercalation of polymers; nevertheless, some characteristic bands of OM, P(2-AT) and PANI overlap, such as the C-C vibrations peaks concealed by the stretching (Si-O) of the clay network located at 1005 cm^{-1}; absorption peaks at around 1509 and 1580 cm^{-1} observed in PANI and PANI-co-P(2-AT) are characteristic of stretching vibration of quinoid and benzenoid rings, respectively [37]; the band at 1741 cm^{-1} attributed to the C=N stretching vibration is shifted to 1546 cm^{-1} in the PANI-co-P(2-AT); an additional band is detected in the two specters of PANI and PANI-co-P(2-AT) at 802 cm^{-1} assigned to the C=C deformation bonds of benzene core, narrow peaks near 2990 cm^{-1} mainly arise from C-H stretching modes; broad peaks observed at 3228 and 3255 cm^{-1} originates from the primary amine N-H vibration of P(2-AT) and PANI, respectively [24], and are merged in the PANI-co-P(2-AT) composite, which appears larger and slightly shifted to 3500 cm^{-1}; in addition, PANI-co-P(2-AT) exhibited additional peaks compared to PANI at 1350 and 1213 cm^{-1} which may correspond to the C-N and the C-S bonds into the thiazole ring. All of these observed spectral peaks confirm the copolymer structure although intensities of most of peaks remained weak due to the restricted growth and limited modes of vibration in synthesized polymers in the presence of OM, since, in situ homo/copolymerization of monomers proceeds between the clay layers after addition of ammonium persulfate.

UV-Vis spectroscopy

In order to investigate optical properties of nanocomposites, UV-Vis spectroscopy was carried out on products. Figure 8 shows the UV-Vis spectra of OM/PANI, OM/P(2-AT), and OM/PANI-co-P(2-AT) nanocomposites. The OM/PANI spectra exhibited an absorption at 332 nm belonging to the polaron-π* transition of benzenoid rings and a second maximum absorption was observed near 641 nm attributed to the π-π* transition

Table 2 Characterized functions bands of OM, OM/P(2-AT), OM/PANI and OM/PANI-co-P(2-AT) nanocomposites

Characterized function	OM (cm^{-1})	OM/P(2-AT) (cm^{-1})	OM/PANI (cm^{-1})	OM/PANI-co-P(2-AT) (cm^{-1})
ν(N—H)	—	3255	3228	3490
ν(C—N)	1471	1280	1200	1284
ν(—C=C—)	—	1530	1527–1490	1510
ν(—C=N—)	—	1710	1590	1750
ν(—C—S—)	—	1209	—	1202
ν(—C—C—)	2847	1180	1104	1159
ν(—C—H)	2877–2905	2952	2910	2980
ν(—Si—O—Mg—)	1005	1005	1005	1005
ν(—O—H)	3625	3625	3625	3625

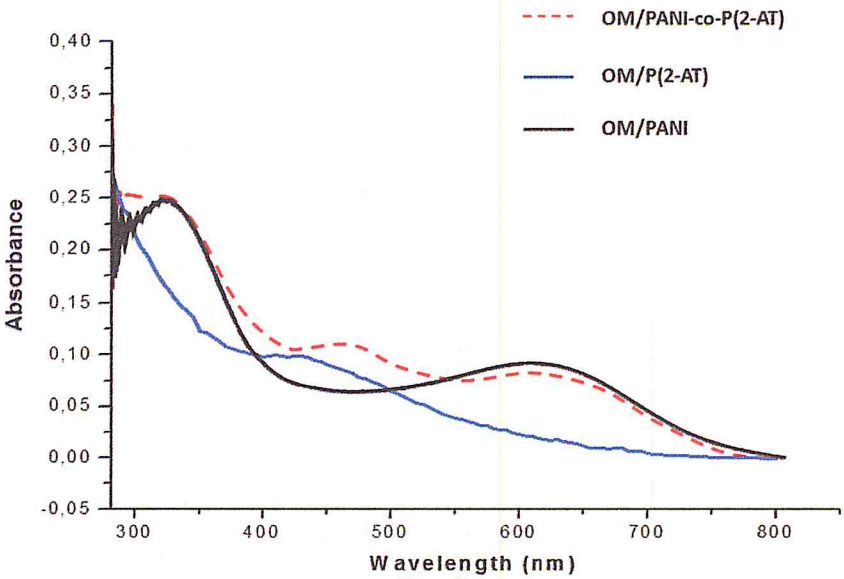

Fig. 8 UV-Vis spectra of OM/PANI, OM/P(2-AT), and OM/PANI-co-P(2-AT) nanocomposites

of the converted aromatic benzenoide rings into quinoides ones [42]. The OM/P(2-AT) nanocomposite spectra shows clearly two major polaron band peaks; at about 280 nm originates from the thiazole ring and at ~439 nm assigned to the conjugated polymer, these results are in good agreement with literature values [43, 44]; in OM/PANI-co-P(2-AT), a large absorption peak between 280 and 350 nm is owing to the fusion of two peaks: (i) 280 nm stemming from the π-π^* transition of thiazole rings and (ii) 340 nm of the benzenoide rings in the PANI chain; we notice that same transitions observed in homopolymers occured in the copolymer; the third band at 475 nm is slightly shifted to higher wavelength followed up with long extending tail shifted to ~650 nm arising from the increased conjugation length in the confined environment of nanoclay layers after the copolymerization.

X-ray diffraction analysis

X-ray diffraction has been used for determining the degree of intercalation and/or exfoliation of the polymer/copolymer matrix in the clay. The XRD patterns of polymer/organ-modified clay nanocomposites compared to OM are shown in Fig. 9 and summarized in Table 3. The OM/P(2-AT) and OM/PANI exhibited a single peak with high intensity around $2\theta = 2.82$–$2.79°$; the oxidative polymerization process occurs obviously between the clay sheets which lead to increase in the basal spacing to an average basal spacing of $d_{001} = 32.12$–32.84 Å, respectively. The diffraction of the OM/PANI-co-P(2-AT) reached lowest value to $2\theta = 2.41°$ which corresponds to d-spacing = 33.9 Å. The interlayer distance of these nanocomposites compared to that of OM nearly doubled. This sharp increase in the platelet length confirms that polymers/copolymer chains were fully inserted within the Maghnite galleries.

Transmission electron microscopy

The TEM images of OM/P(2-AT), OM/PANI, and OM/PANI-co-P(2-AT) nanocomposites are shown in Fig. 10a–c. In these three images, it is clearly observed that the layers of the clay indicate that the polymers are intercalated in these layers. These TEM results were in good agreement with the results of the XRD patterns.

Thermogravimetric analysis

Thermogravimetric (TG) analysis was used to investigate thermal stability of the mineral organoclay and its

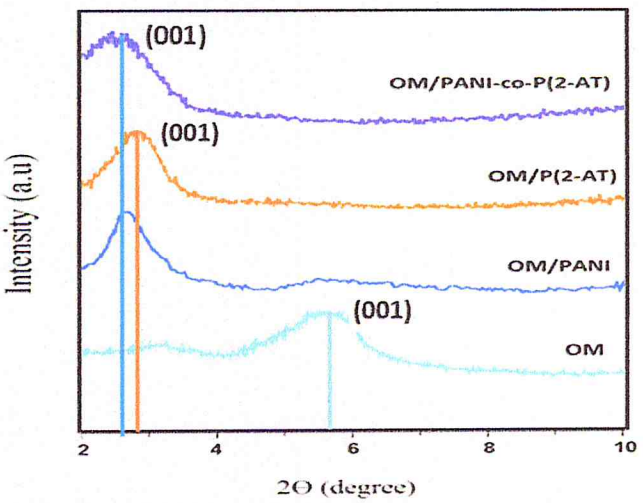

Fig. 9 X-ray diffraction patterns of OM, OM/PANI, OM/P(2-AT), and OM/PANI-co-P(2-AT) nanocomposites

t3.1 **Table 3** Peak maximum and *d*-spacing of OM, OM/PANI, OM/P(2-AT), and OM/PANI-co-P(2-AT) nanocomposite

Samples	Peak max 20 max (degree)	Basal spacing *d*(001) (Å)	Interlayer spacing, Δd (Å)
Raw-M	7.81	11.9	–
M-Na+	7.42	12.45	0.55
OM	5.45	19.14	6.69
OM/P(2-AT)	2.82	32.12	12.98
OM/PANI	2.79	32.84	1.72
OM/PANI-co-P(2-AT)	2.41	33.9	1.06

nanocomposites. The TG curves in Fig. 11 furnished several information on the structure of the modified clay, it showed significantly weight loss behavior, the major mass loss of M-Na^+ was about 15% and occurred at 180 °C; this mass decrease is associated to the loss of adsorbed water molecules surrounding compensating cations between the clay sheets, while the mass loss rate observed for OM was smaller, reflecting the hydrophobic behavior of the organo-modified clay, since the interlayer water was integrally substituted by the inserted cationic surfactant. The principal weight loss for organophilic Maghnite recorded at 312 °C is obviously due to the disappearance of HCl molecules accompanied with total decomposition of the cationic surfactant content into the Maghnite layer which degrades beyond 503 °C [45]. The process of decomposition of nanocomposites is almost similar to that of the OM, it occurred in several steps; OM/PANI has a wide decomposition peak near 568 °C, whereas, OM/PANI-co-(2-AT) and OM/P(2-AT) have only one large peak between 500 °C and 680 °C, which probably corresponds to the elimination of low molecular weight fragments followed by complete degradation of the polymer matrix beyond 700 °C; it is well known that the extend in the length of the chain leads to an increase in the interval of decomposition. The obtained results confirm that the inorganic cations has been substituted and replaced by the cationic surfactant and the polymer/copolymer chains, in conclusion, the thermal stability raising of nanocomposites/ incorporated clays is due to the barrier properties of Maghnite particles for the mass transportation throughout the decomposition process and extensively enhanced the thermal stability of materials.

Measurement of the electrical conductivity

Table 4 shows the electrical conductivities of PANI, P(2-AT), and PANI-co- P(2-AT) measured by Hall effect on a glass substrate,; after the polymers were extracted from the clay, the solutions were cast over on the substrate; then, the solvent was evaporated to create a thin layer of polymers [46, 47]. The specific conductivity of the polymers was measured with direct current from 5 to 25 V; in this range, the samples showed Ohmic behaviors and were found to be about 2.766×10^{-7} $S.cm^{-1}$ for PANI and 1.966×10^{-7} $S.cm^{-1}$ for P(2-AT) which increased up to about 10^{-3} $S.cm^{-1}$ upon doping of the polymer with I_2 [20] and 9.951×10^{-7}S/cm for PANI-co-P(2-

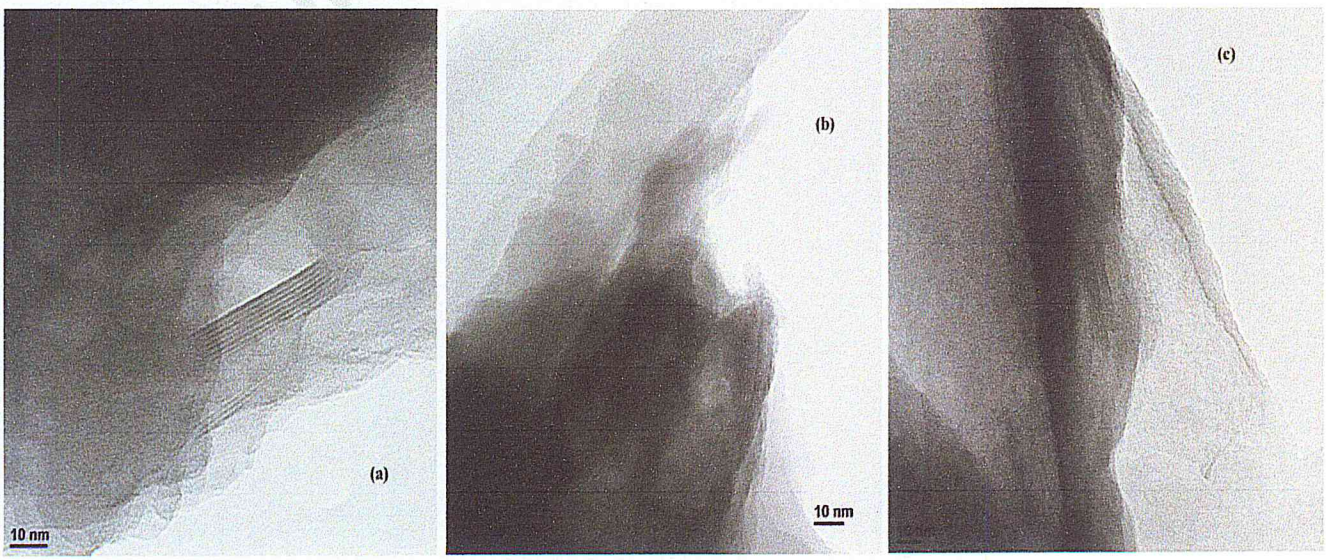

Fig. 10 TEM images of a OM/P(2-AT), b OM/PANI, and c OM/PANI-co-P(2-AT) nanocomposites

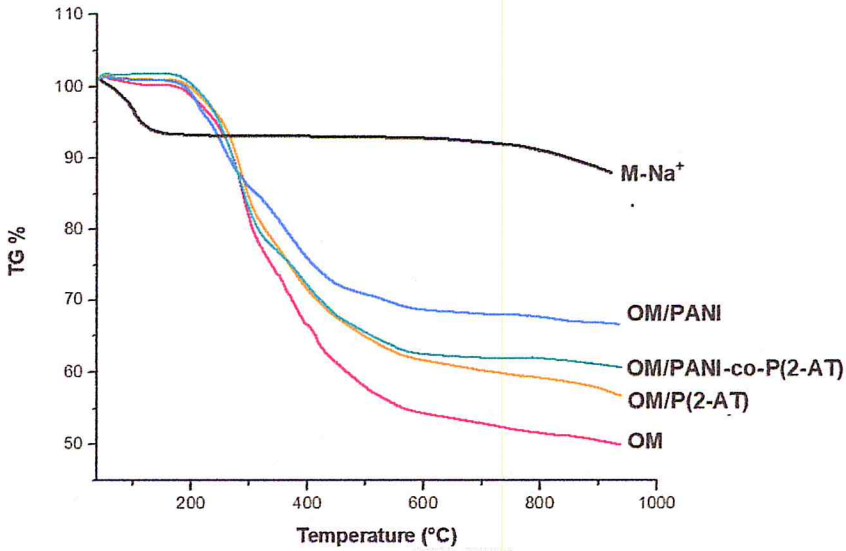

Fig. 11 Thermogravimetric analysis (TG) of M-Na^+, OM, OM/PANI, OM/P(2-AT), and OM/PANI-co-P(2-AT) nanocomposites

AT) which is higher than that of homopolymers, probably due to the increased conjugation length after the copolymerization.

Conclusion

This paper attempts to present a method for the fabrication of clay/polymer nanocomposites based on organophilic clay. The cetrimonium bromide (CTAB) has been exchanged with sodium cations from the Maghnite clay; the intercalation of the cationic surfactant within the Maghnite interlayer spacing has been investigated by FTIR, DRX, and XPS. The monomers and co-monomers were polymerized by in situ oxidative polymerization in aqueous solution with stoichiometric amount of ammonium persulfate and largely incorporated into the organo-modified clay. The polymer yield increased with increasing polymerization time and oxidant amount up to a certain value, the intercalated nanocomposites structure was investigated by FTIR, UV-Vis, DRX, ATG, XPS, and Hall effect measurement. FTIR indicates that there is strong interactions between polymer/copolymer chains and the organophilic Maghnite, UV-Vis spectroscopy and X-ray diffraction showed some peaks shifts which reveals that nanocomposites have well-intercalated structures, Good electrical response has been observed of extracted polymers/copolymer from the composites indicates that the polymerization into Organophilic clay produces electroactive polymers, thermal stability of synthesized nanocomposites increased due to the barrier properties of clays.

Table 4 Electrical conductivity of PANI, P(2-AT), and PANI-co-P(2-AT)

Sample	Original ($S.cm^{-1}$)
PANI	2.766×10^{-7}
P(2-AT)	1.966×10^{-7}
PANI-co-P(2-AT)	9.951×10^{-7}

Acknowledgments Special thanks are given to Professeur A. Khelil and Dr. Y. Mouchaal for the electrical measurement.

Funding This work was financially supported by the Agency Thematic Research Science and Technology (ATRST), the Directorate General of Scientific Research and Technological Development (La Direction Générale de la Recherche Scientifique et du Développement Technologique (DGRSDT)) of Algeria.

Compliance with ethical standards

Conflict of interest They have no conflict of interest.

References

1. Lee HW, Karim MR, Ji HM, Choi JH, Ghim HD, Park JH, Oh W, Yeum JH (2009) Electrospinning fabrication and characterization of poly(vinyl alcohol)/montmorillonite nanofiber mats. J Appl Polym Sci 113:1860–1867
2. Alcântara ACS, Darder M, Aranda P, Ayral A, Ruiz-Hitzky E (2015). J Appl Polym Sci 133:54
3. Schnitzler DBC, Meruvia MS, Hummelgen IA, Zarbin AJG (2003). Chem Mater 15:4658
4. Zare Y, Shabani I (2016) Polymer/metal nanocomposites for biomedical applications. Mater Sci Eng 60:195–203
5. Jafari M, Rahimi A, Shokrolahi P, Langroudi AE (2014) Synthesis of antistatic hybrid nanocomposite coatings using surface modified indium tin oxide (ITO) nanoparticles. J Coat Technol Res 11:587–593
6. Hosseini MG, Raghibi-Boroujeni M, Ahadzadeh I, Najjar R, Dorraji MSS (2009) Effect of polypyrrole–montmorillonite nanocomposites powder addition on corrosion performance of epoxy coatings on Al 5000. Prog Org Coat 66:321–327
7. Silva RC, Sarmento MV, Nogueira FAR, Tonholo J, Mortimer RJ, Faez R, Ribeiro AS (2014) Enhancing the electrochromic response of polyaniline films by the preparation of hybrid materials based on

polyaniline, chitosan and organically modified clay. RSC Adv 4: 14948–14955
8. Mahore RP, Burghate DK, Kondawar SB (2014) Development of nanocomposites based on polypyrrole and carbon nanotubes for supercapacitors. Adv Mater Lett 5:400–405
9. Rivero RE, Molina MA, Rivarola CR, Barbero CA (2014) Pressure and microwave sensors/actuators based on smart hydrogel/conductive polymer nanocomposite. Sensors Actuators B Chem 190:270–278
10. Yahiaoui A, Belbachir M, Hachemaoui A (2009) Cationic polymerization of ethylene oxide with Maghnite-H as a clay catalyst in the presence of ethylene glycol. J Appl Polym Sci 113:535–540
11. Hachemaoui A, Belbachir M, Yahiaoui A (2011). J Appl Polym Sci 115:3445
12. Ghosh S, Sannigrahi A, Maity S, Jana T (2011). J Phys Chem 115: 11474
13. Salmi Z, Benzarti K, Chehimi M, Langmuir M (2013) Diazonium cation-exchanged clay: an efficient, unfrequented route for making clay/polymer nanocomposites 29:13323–13328
14. Boufatit MM, Ait-Amar H, Mc Whinnie WR (2008) Development of an Algerian material montmorillonite clay — intercalation with selective long chain alkylammonium cations (octadecytrimethylammonium, cetylpyridium and tetrabutylammonium) and with tellerium complexes development of an algerian material montmorillonite. Desalination. 223:366–374
15. Biswas M, Ray SS (2001) Recent progress in synthesis and evaluation of polymer-montmorillonite nanocomposites. Adv Polym Sci 155:167
16. Abd El-Ghaffar MA, Youssef AM, Abd El-Hakim AA (2015) Polyaniline nanocomposites via in situ emulsion polymerization based on montmorillonite: preparation and characterization. Arab J Chem 8:771–779
17. Park SJ, Seo DA, Lee JR (2002) Surface modification of montmorillonite on surface acid–base characteristics of clay and thermal stability of epoxy/clay nanocomposites. J Colloid Interface Sci 251:160–165
18. Sayyah SM, Kamal SM, Abd El-Rehim SS (2006) Electrochemical polymerization of 2-amino-4-(4-methoxyphenyl)thiazole and characterization of the obtained polymer. J Polym Mater 55:79–101
19. Sayyah SM, EL-Deeb SM, Abdel-Rehim SS (2004) Electropolymerization of 2-amino-4-phenylthiazole and characterization of the obtained polymer films. J Polym Mater 53:941–958
20. Ciftci H, Testereci HN, Oktem Z (2013) Ring opening polymerization of 2-aminothiazole with iron(III) chloride. Polym Bull 70: 1895–1909
21. Dubrovskii RA, Aksimenteva EI (2008) Anodic synthesis and properties of polyaminothiazole. Russ J Electrochem 44:234–237
22. Catellani M, Destri S, Porzio W (1988) Thiazole-based polymers: Synthesis, characterization and electronic structure. Synth Met 26: 259–265
23. Zou H, Wu D, Sun H, Chen S, Wang X (2018) Poly(2-aminothiazole)-silica nanocomposite particles: synthesis and morphology control. Appl Surf Sci 436:1083–1092
24. Wang X, Lv PF, Zou H, Li Y, Li XY, Liao YZ (2016) Synthesis of poly(2-aminothiazole) for selective removal of Hg(II) in aqueous solutions. Ind Eng Chem Res 55:4911–4918
25. MacDiarmid AG, Epstein A (1994) The concept of secondary doping as applied to polyaniline. J Synthetic Met 65:103–116
26. Sherman BC, Euler WB, Force RR (1994). J Chem Educ 4:A94
27. Abu-Thabit YN (2016) Chemical oxidative polymerization of polyaniline: a practical approach for preparation of smart conductive textiles. J Chem Educ 93:1606–1611
28. Embarek N, Sahli N, Belbachir M (2019) Preparation and characterization of poly(3-glycidoxypropyltrimethoxysilane) nanocomposite using organophilic montmorillonite clay (Magcetyltrimethylammonium). J Compos Mater 53:4313–4322
29. Mravcakova M, Boukerma K, Omastova M, Chehimi MM (2006) Montmorillonite/polypyrrole nanocomposites. The effect of organic modification of clay on the chemical and electrical properties. Mater Sci Eng 26:306–313
30. Hoang VH, Holze R (2006) Electrochemical synthesis of polyaniline/montmorillonite nanocomposites and their characterization. Chem Mater 18:1976–1980
31. Yahiaoui A, Belbachir M, Hachemaoui A (2003). Int J Mol Sci 4: 548
32. Lee D, Lee SH, Char K, Kim J (2000) Expansion distribution of basal spacing of the silicate layers in polyaniline/Na+-montmorillonite nanocomposites monitored with X-ray diffraction. Macromol Rapid Commun 21:1136–1139
33. Tiffour I, Bassaid S, Dehbi A, Belfedal A, Mourad A-H-I, Zeinert A (2019). Surf Rev Lett 26:1850127
34. Tiffour I, Dehbi A, Mourad A-H-I, Belfedal A (2016). Mater Chem Phys 178:49
35. Gherrass H, Hachemaoui A, Yahiaoui A, Belfadel A, Dehbi A, Mourad A-H-I (2018). J Semicond 39:102001
36. Bonczek JL, Harris WG, Nkedi-Kizza P (2002). Clay Clay Miner 50:7
37. Nascimento GM, Constantino VRL, Landers R, Temperini MLA, Chen SA, Lee HT (2004) Aniline polymerization into montmorillonite clay: a spectroscopic investigation of the intercalated conducting polymer. Macromolecules. 37:9373–9385
38. Lagaly G (1986) Interaction of alkylamines with different types of layered compounds. Solid State Ionics 22:43–51
39. Chen D, Chen J, Luan X, Ji H, Xia Z (2011) Characterization of anion–cationic surfactants modified montmorillonite and its application for the removal of methyl orange. Chem Eng J 171:1150–1158
40. Mao H, Li B, Li X, Yue L, Liu Z, Ma W (2010) Novel one-step synthesis route to ordered mesoporous silica-pillared clay using cationic–anionic mixed-gallery templates. Ind Eng Chem Res 49: 583–591
41. Tahani A, Karroua M, Van Damme H, Levitz P, Bergaya F (1999) Adsorption of a cationic surfactant on Na–montmorillonite: inspection of adsorption layer by X-ray and fluorescence spectroscopies. J Colloid Interface Sci 216:242–249
42. Hua MY, Hwang GW, Chuang YH, Chen SA, Tsai RY (2000) Soluble n-doped polyaniline: synthesis and characterization. Macromolecules. 33:6235–6238
43. Imamoglu T, Onal AM (2007). J Eur Polym 40:1875
44. Solmaz R, Kardas G (2009) Electrochemical synthesis and characterization of poly-2-aminothiazole. Prog Org Coat 64:81–88
45. Hattab Y, Benharrats N (2015) Thermal stability and structural characteristics of PTHF–Mmt organophile nanocomposite. Arab J Chem 8:285–292
46. Gherras H, Yahiaoui A, Hachemaoui A, Belfedal A, Dehbi A, Zeinert A (2019). Polym Polym Compos. https://doi.org/10.1177/0967391119872876
47. Bouabida NH, Hachemaoui A, Yahiaoui A, Gherras H, Belfedal A, Dehbi A, Mourad A-HI (2020). Polymer Sci Ser B 62(2):163
48. Greiner A, Wendorff JH (2007). Angew Chem Int Ed 46(30):5670